molecules

MDPI

Article

$B_3Al_4^+$: A Three-Dimensional Molecular Reuleaux Triangle

Li-Xia Bai [1], Mesías Orozco-Ic [2,*], Ximena Zarate [3], Dage Sundholm [2], Sudip Pan [4], Jin-Chang Guo [1,*] and Gabriel Merino [5,*]

1 Nanocluster Laboratory, Institute of Molecular Science, Shanxi University, Taiyuan 030006, China
2 Department of Chemistry, University of Helsinki, A. I. Virtasen Aukio 1, P.O. Box 55, FIN-00014 Helsinki, Finland
3 Instituto de Ciencias Químicas Aplicadas, Facultad de Ingeniería, Universidad Autónoma de Chile, Av. Pedro de Valdivia 425, Santiago 7500912, Chile
4 Fachbereich Chemie, Philipps-Universitt Marburg Hans-Meerwein-Straße, 35043 Marburg, Germany
5 Departamento de Física Aplicada, Centro de Investigación y de Estudios Avanzados, Unidad Mérida. Km 6 Antigua Carretera a Progreso. Apdo., Postal 73, Cordemex, Merida 97310, Mexico
* Correspondence: mesias.orozcoic@helsinki.fi (M.O.-I.); guojc@sxu.edu.cn (J.-C.G.); gmerino@cinvestav.mx (G.M.)

Abstract: We systematically explore the potential energy surface of the $B_3Al_4^+$ combination of atoms. The putative global minimum corresponds to a structure formed by an Al_4 square facing a B_3 triangle. Interestingly, the dynamical behavior can be described as a Reuleaux molecular triangle since it involves the rotation of the B_3 triangle at the top of the Al_4 square. The molecular dynamics simulations, corroborating with the very small rotational barriers of the B_3 triangle, show its nearly free rotation on the Al_4 ring, confirming the fluxional character of the cluster. Moreover, while the chemical bonding analysis suggests that the multicenter interaction between the two fragments determines its fluxionality, the magnetic response analysis reveals this cluster as a true and fully three-dimensional aromatic system.

Keywords: boron clusters; fluxionality; aromaticity

check for updates

Citation: Bai, L.-X.; Orozco-Ic, M.; Zarate, X.; Sundholm, D.; Pan, S.; Guo, J.-C.; Merino, G. $B_3Al_4^+$: A Three-Dimensional Molecular Reuleaux Triangle. *Molecules* **2022**, *27*, 7407. https://doi.org/10.3390/molecules27217407

Academic Editors: Felipe Fantuzzi and Marco A. C. Nascimento

Received: 22 September 2022
Accepted: 23 October 2022
Published: 1 November 2022

1. Introduction

In 2010, Wang and coworkers detected an anionic cluster of nineteen boron atoms in the gas phase through a photoelectron spectroscopy experiment [1]. The structure has a planar pentagonal inner B_6 core encircled by a B_{13} ring (Figure 1a). A couple of years later, Merino and coworkers found that the inner B_6 fragment rotates almost freely with respect to the periphery [2], so they labeled this type of system as a Wankel-type rotor [2–8]. Over time, other boron clusters were also reported to exhibit similar behavior, including B_{13}^+ as the most prominent case [9,10]. In fact, the dynamic behavior of B_{13}^+ was experimentally verified by Asmis et al. in 2016 using cryogenic ion vibrational spectroscopy [11,12]. The main reason for this fascinating fluxionality is attributed to the multicenter bonds, often found in boron clusters [13]. Moreover, this property is not exclusive to only planar forms; compasses [14,15], drums [16], stirrers, sphere-shaped clusters [17], and other doped boron architectures have similar dynamic behavior [18–21]. Other related examples are the global minima of B_7M_2 and B_8M_2 (M = Zn, Cd, Hg), which can be described as an M_2 dimer spinning freely on a boron wheel resembling a magnetic stirrer placed on a baseplate [22]. The reader interested in more details on fluxionality in boron clusters is referred to [12].

Inspired by these fluxional boron systems, we analyze the dynamical properties of the global minimum of $B_3Al_4^+$ (Figure 1b). This cluster has an Al_4 square facing a B_3 triangle. Although this system was recently reported by Wen et al. [23], they overlooked its fluxional properties. Moreover, upon further exploration of the nature of the bonding and aromaticity, we find that this system has all the characteristics to define it as a true and fully three-dimensional aromatic system.

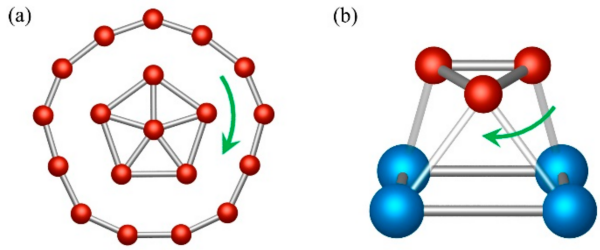

Figure 1. (**a**) The Wankel rotor B_{19}^- and (**b**) Three-dimensional molecular Reuleaux triangle $B_3Al_4^+$.

2. Computational Details

The PES was systematically explored using the Coalescence Kick (CK) program and a modified genetic algorithm implemented in GLOMOS [24,25]. Initial screening in singlet and triplet states was performed for both programs at the PBE0/LAN2DZ level [26,27]. In the range of 30 kcal mol^{-1} above the putative global minimum, the lowest isomers were minimized and characterized at the PBE0/def2-TZVP level [28]. Final energies were computed at the CCSD(T) [29]/def2-TZVP level, including the zero-point energy correction (ZPE) at the PBE0/def2-TZVP level. Thus, the energy discussion is based on the CCSD(T)/def2-TZVP//PBE0/def2-TZVP results. Natural bond orbital analysis was conducted at the PBE0 level to obtain natural atomic charges (using the NBO6 program [30]) and Wiberg bond indices (WBI) [31]. The Born–Oppenheimer molecular dynamics [32] (BOMD) were carried out at the PBE0/6-31G(d) level to ascertain the fluxional behavior. The aromatic character was evaluated by computing the magnetic response to a uniform external magnetic field. This is achieved by calculating the magnetically induced current density [33–36] ($\mathbf{J}^{ind}$) and the induced magnetic field [37–39] ($\mathbf{B}^{ind}$) using the GIMIC [33–36] and Aromagnetic [40] programs, respectively. Since magnetic properties computed with the BHandHLYP [41] functional yield results in good agreement with those obtained by CCSD(T) computations [42], $\mathbf{J}^{ind}$ and $\mathbf{B}^{ind}$ were calculated at the BHandHLYP/def2-TZVP level using gauge-including atomic orbitals (GIAOs) [43,44]. All these calculations were performed with Gaussian 16 [45]. Furthermore, the adaptive natural density partitioning [46] (AdNDP) analysis was also carried out to understand the nature of the interactions using the Multiwfn program [47].

3. Discussion

The putative global minimum of $B_3Al_4^+$ is a singlet with C_s symmetry (**1**), in which an Al_4 square interacts with a B_3 triangle, forming a polyhedron (see Figure 2). The B-B distances range from 1.60–1.63 Å, creating an isosceles triangle with a B-B bond aligned with an Al-Al bond. On the other hand, the Al_4 ring is a trapezoid or quasi-square, with Al-Al bond distances lying between 2.60–2.77 Å. The distance between the two fragments is 1.73 Å.

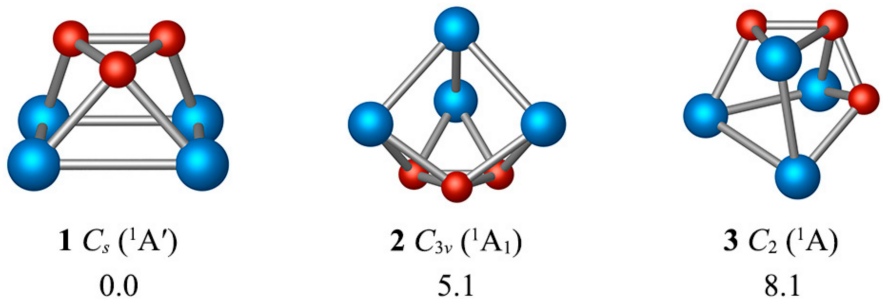

Figure 2. PBE0/def2-TZVP structures of the three lowest-lying energy isomers of $B_3Al_4^+$.

The energetically closest isomer is only 5.1 kcal mol^{-1} above the global minimum and consists of an Al_4 tetrahedron. The third isomer differs from the putative global minimum by exchanging a B atom for an Al atom and is 8.1 kcal/mol higher in energy. Note that

all isomers in Figure S1 have a B_3 unit. As shown in Figure S2, the lowest vibrational frequency of **1** is 69 cm^{-1}, which corresponds to the rotation of the B_3 fragment. Following this smooth rotation mode, we identify the transition state (TS) belonging to the C_s point group. The structural variations between the TS and the global minimum are negligible. The rotation barrier is only 0.1 kcal/mol (including the zero-point energy correction), which means that the B_3 ring can undergo almost free rotation on top of the Al_4 ring.

Figure 3 shows the structural evolution of $B_3Al_4^+$ with the B_3 triangle rotating clockwise. Starting from the global minimum, fragment B_3 must rotate 15° to reach the maximum of the rotation barrier. A new minimum is achieved by rotating B_3 another 15°, and a complete rotation lap is obtained by repeating this process twelve times. BOMD simulations at 300 K for 25 ps and starting from the global minimum structure show that the B_3 triangle rotates with respect to the Al_4 ring, just like a three-dimensional (3D) molecular Reuleaux triangle. The average distance between the B_3 triangle and the Al_4 quasi-square remains constant (see Movie 1 in the supplementary material).

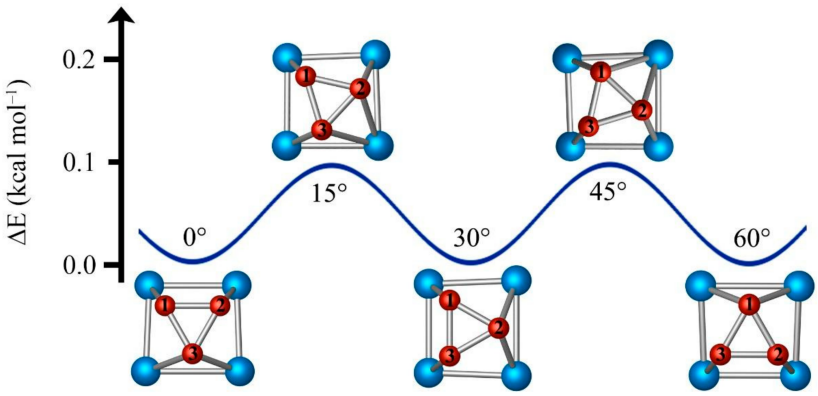

Figure 3. Structural evolution of three-dimensional molecular Reuleaux triangle $B_3Al_4^+$ during the dynamic rotation.

A chemical bonding analysis is crucial to understanding the dynamical behavior of $B_3Al_4^+$. The natural atomic charges and WBIs for **1** and TS are shown in Figure S3. The charge distribution is such that the B_3 fragment has a charge of −2.0 |e| and the Al_4 moiety of 3.0|e|. Instead, the WBI values show that the B-B bonds (WBI around 1.1) have a higher covalent character than the Al-Al bonds (WBI between 0.32 and 0.65), but even more fascinating is that the WBI values for the B-Al bonds are of the same magnitude as the latter (0.49 and 0.62), indicating that there is significant orbital overlap (an electron delocalization) between both fragments. We also employed AdNDP, an extension of the NBO analysis. AdNDP analysis recovers not only Lewis bond elements (lone pairs and 2c-2e bonds) but also multicenter bonds (nc-2e, $n \geq 3$). For $B_3Al_4^+$, the analysis identifies three 3c-2e σ-bonds with occupation numbers (ON) of 1.99–1.83 |e| and one π-bond (ON = 1.71 |e|) located mainly throughout the B_3 fragment. This electron distribution is like that reported for the aromatic cyclopropenyl cation ($C_3H_3^+$). On the other hand, the Al_4 ring has three 4c-2e σ-bonds with ON of 1.99–1.88 |e|. The B_3 triangle and the Al_4 trapezoid interact via three 7c-2e bonds (Figure 4). Thus, the absence of 2c-2e bonds between the two fragments favors free rotation [48]. The bonding pattern for the TS is similar to that of the global minimum, as shown in Figure S4. The orbital compositions of canonical molecular orbitals (CMOs) for **1** and TS are listed in Tables S1 and S2, which support the bonding pattern provided by AdNDP.

As shown in Figure S5, the B_3 ring has six σ- and two π-electrons, i.e., in principle, it satisfies Hückel's aromaticity rule for both the σ- and π-clouds. Now, while the Al_4 ring has six electrons, which we could classify as σ, the region between the two rings is also connected via six electrons, so both the Al_4 fragment and the area between the rings satisfy the Hückel's rule. The reality is that the orbital separation is complicated, and all the bonds in $B_3Al_4^+$ have a multicentric character, i.e., they are fully delocalized in the small cage.

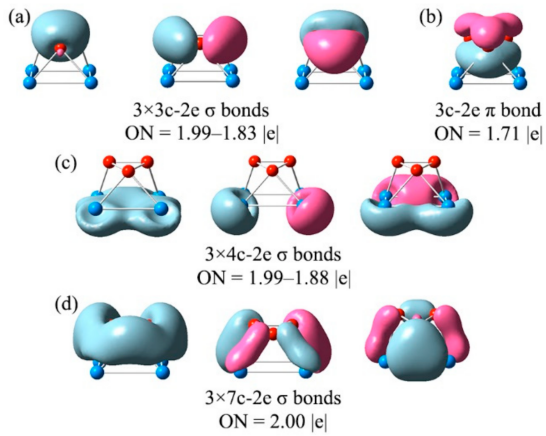

Figure 4. The adaptive natural density partitioning (AdNDP) bonding pattern for $B_3Al_4^+$ (GM). ON is the occupation number.

Aromaticity of $B_3Al_4^+$ is confirmed by its magnetic response to an external magnetic field perpendicular to the Al_4 ring. The $\mathbf{B}^{ind}$ analysis reveals strong shielding values (<−50 ppm) of the *z*-component of $\mathbf{B}^{ind}$ ($B^{ind}{}_z$) along the region between the Al_4 and B_3 rings. This can be explained by the presence of an entirely diatropic current density in this region (Figure 5a). Thus, the interaction of both rings creates a ring current in the region between the two rings instead of being two separate ring currents, implying that $B_3Al_4^+$ has true three-dimensional aromaticity (Figure 5b). Integration of $\mathbf{J}^{ind}$ in a plane that intersects the Al-Al and B-B bonds yields a ring–current strength (J^{ind}) of 33.3 nA/T. Changes in the current density can be obtained by calculating the spatial derivative of the ring–current strength along the vertical *z*-axis (dJ^{ind}/dz) [49]. This indicates that there are no paratropic contributions along the *z*-profile. Additionally, the ring–current profile shows that the strongest current density flux occurs just below the boron triangle, confirming the three-dimensional delocalization along the *z*-axis (Figure S6 in Supporting Information). Thus, $B_3Al_4^+$ is a true 3D aromatic fluxional cluster.

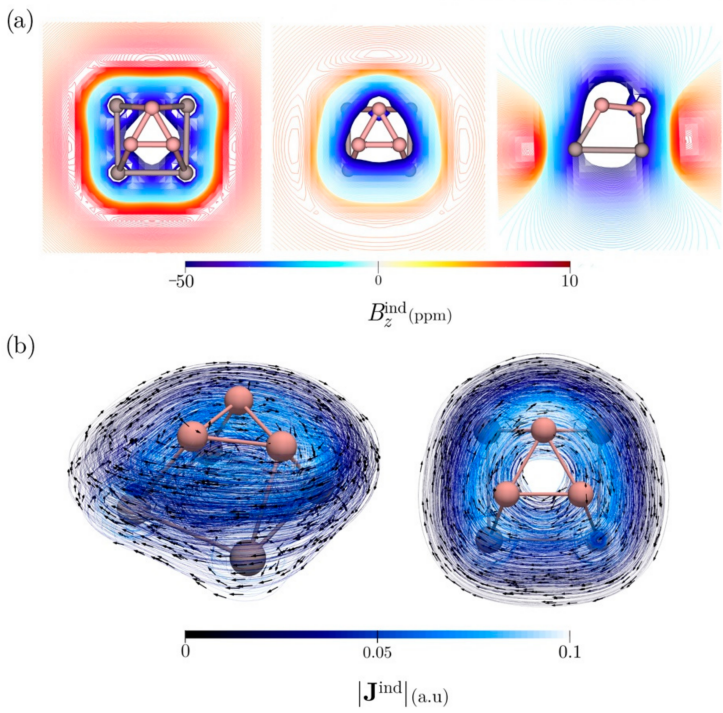

Figure 5. (**a**) $B^{ind}{}_z$ isolines plotted in the plane of the Al_4 framework (**left**), the B triangle (**middle**), and in a transverse plane (**right**) to $B_3Al_4^+$. (**b**) $\mathbf{J}^{ind}$ vector maps plotted near $B_3Al_4^+$. The arrows

indicate the direction of the current density. The $|\mathbf{J}^{ind}|$ scale is in atomic units (1 au = 100.63 nA/T/Å^2). The external magnetic field is oriented parallel to the *z*-axis, perpendicular to the Al_4 plane.

4. Summary

After systematically exploring the potential energy surface of clusters with formula $B_3Al_4^+$, we confirm that the putative global minimum corresponds to a structure formed by an Al_4 quasi-square facing a B_3 triangle. Most interestingly, the global minimum of $B_3Al_4^+$ exhibits fluxionality. However, its dynamic behavior involves the rotation of the B_3 triangle on the Al_4 ring, embodying a molecular Reuleaux triangle. Corroborated by BOMD, a complete rotation cycle includes twelve repeating steps comprising the global minimum and a transition state separated by only 0.1 kcal/mol, indicating that the rotation between both fragments is virtually free. Furthermore, the AdNDP analysis suggests that the interaction between the B and Al fragments is via three 7c-2e bonds, favoring such dynamical behavior. Regarding aromaticity, the analysis based on the magnetic response reveals a strong shielding along the *z*-axis due to an entirely diatropic current density flowing between fragments leading to a three-dimensional double ($\sigma + \pi$)-aromaticity. So, we find a peculiar three-dimensional fluxional 3D aromatic cluster that resembles a molecular Reuleaux triangle.

Supplementary Materials: The following supporting information can be downloaded at: https://www.mdpi.com/article/10.3390/molecules27217407/s1, Figure S1: Twenty low-lying isomers of $B_3Al_4^+$; Figure S2: Displacement vectors of soft vibrational mode of the global minimum and TS; Figure S3: Computed bond distances, Wiberg bond indices, and natural atomic charges for both the global minimum and TS of $B_3Al_4^+$; Figure S4: Bonding pattern, according to AdNDP analysis, in the transition state related to the rotation of the B3 fragment in $B_3Al_4^+$; Figure S5: Bonding model for $B_3Al_4^+$; Figure S6: The vertical ring-current profile along the z-axis; Tables S1 and S2: Orbital composition analysis for occupied canonical molecular orbitals for both the global minimum and transition state of $B_3Al_4^+$; Video S1: Molecular dynamics of $B_3Al_4^+$; Cartesian coordinates of both the global minimum and the transition state.

Author Contributions: Conceptualization, J.-C.G. and G.M.; validation, L.-X.B., S.P. and X.Z.; writing, S.P., M.O.-I., D.S., J.-C.G. and G.M. All authors have read and agreed to the published version of the manuscript.

Funding: This work was supported by the National Natural Science Foundation of China (22173053) and the Natural Science Foundation of Shanxi Province (20210302123439). This work was funded in Mexico by Conacyt (Proyecto Sinergia 1561802). The work in Finland was supported by the Academy of Finland (Project numbers 314821 and 340583), the Magnus Ehrnrooth Foundation, Waldemar von Frenckell's Foundation, and the Swedish Cultural Foundation in Finland.

Institutional Review Board Statement: Not applicable.

Informed Consent Statement: Not applicable.

Data Availability Statement: Not applicable.

Conflicts of Interest: The authors declare no conflict of interest.

Sample Availability: Samples of the compounds are not available from the authors.

References

1. Huang, W.; Sergeeva, A.P.; Zhai, H.-J.; Averkiev, B.B.; Wang, L.-S.; Boldyrev, A.I. A concentric planar doubly π-aromatic B_{19}^- cluster. *Nat. Chem.* **2010**, *2*, 202–206. [CrossRef] [PubMed]
2. Jiménez-Halla, J.O.C.; Islas, R.; Heine, T.; Merino, G. B_{19}^-: An aromatic Wankel motor. *Angew. Chem. Int. Ed. Engl.* **2010**, *49*, 5668–5671. [CrossRef]
3. Moreno, D.; Pan, S.; Zeonjuk, L.L.; Islas, R.; Osorio, E.; Martínez-Guajardo, G.; Chattaraj, P.K.; Heine, T.; Merino, G. B_{18}^{2-}: A quasi-planar bowl member of the Wankel motor family. *Chem. Commun.* **2014**, *50*, 8140–8143. [CrossRef]

4. Wang, Y.-J.; Zhao, X.-Y.; Chen, Q.; Zhai, H.-J.; Li, S.-D. B_{11}^-: A moving subnanoscale tank tread. *Nanoscale* **2015**, *7*, 16054–16060. [CrossRef]
5. Wang, Y.-J.; You, X.-R.; Chen, Q.; Feng, L.-Y.; Wang, K.; Ou, T.; Zhao, X.-Y.; Zhai, H.-J.; Li, S.-D. Chemical bonding and dynamic fluxionality of a B_{15}^+ cluster: A nanoscale double-axle tank tread. *Phys. Chem. Chem. Phys.* **2016**, *18*, 15774–15782. [CrossRef]
6. Yang, Y.; Jia, D.; Wang, Y.-J.; Zhai, H.-J.; Man, Y.; Li, S.-D. A universal mechanism of the planar boron rotors B_{11}^-, B_{13}^+, B_{15}^+, and B_{19}^-: Inner wheels rotating in pseudo-rotating outer bearings. *Nanoscale* **2017**, *9*, 1443–1448. [CrossRef]
7. Liu, L.; Moreno, D.; Osorio, E.; Castro, A.C.; Pan, S.; Chattaraj, P.K.; Heine, T.; Merino, G. Structure and bonding of IrB_{12}^-: Converting a rigid boron B_{12} platelet to a Wankel motor. *RSC Adv.* **2016**, *6*, 27177–27182. [CrossRef]
8. Wang, Y.-J.; Feng, L.-Y.; Zhai, H.-J. Starting a subnanoscale tank tread: Dynamic fluxionality of boron-based $B_{10}Ca$ alloy cluster. *Nanoscale Adv.* **2019**, *1*, 735–745. [CrossRef] [PubMed]
9. Martínez-Guajardo, G.; Sergeeva, A.P.; Boldyrev, A.I.; Heine, T.; Ugalde, J.M.; Merino, G. Unravelling phenomenon of internal rotation in B_{13}^+ through chemical bonding analysis. *Chem. Commun.* **2011**, *47*, 6242–6244. [CrossRef] [PubMed]
10. Merino, G.; Heine, T. And yet it rotates: Thestarter for a molecular Wankel motor. *Angew. Chem. Int. Ed. Engl.* **2012**, *51*, 10226–10227. [CrossRef]
11. Fagiani, M.R.; Song, X.; Petkov, P.; Debnath, S.; Gewinner, S.; Schöllkopf, W.; Heine, T.; Fielicke, A.; Asmis, K.R. Structure and fluxionality of B_{13}^+ probed by infrared photodissociation spectroscopy. *Chem. Int. Ed. Engl.* **2017**, *56*, 501–504. [CrossRef]
12. Pan, S.; Barroso, J.; Jalife, S.; Heine, T.; Asmis, K.R.; Merino, G. Fluxional boron clusters: From theory to reality. *Acc. Chem. Res.* **2019**, *52*, 2732–2744. [CrossRef]
13. Jalife, S.; Liu, L.; Pan, S.; Cabellos, J.L.; Osorio, E.; Lu, C.; Heine, T.; Donald, K.J.; Merino, G. Dynamical behavior of boron clusters. *Nanoscale* **2016**, *8*, 17639–17644. [CrossRef]
14. Wang, Y.-J.; Feng, L.-Y.; Guo, J.-C.; Zhai, H.-J. Dynamic Mg_2B_8 cluster: A nanoscale compass. *Chem. Asian J.* **2017**, *12*, 2899–2903. [CrossRef]
15. Zhang, X.-Y.; Guo, J.-C. Dynamic fluxionality of ternary Mg_2BeB_8 cluster: A nanocompass. *J. Mol. Model.* **2020**, *26*, 30. [CrossRef]
16. Li, W.-L.; Jian, T.; Chen, X.; Li, H.-R.; Chen, T.-T.; Luo, X.-M.; Li, S.-D.; Li, J.; Wang, L.-S. Observation of a metal-centered B_2-Ta@B_{18}^- tubular molecular rotor and a perfect Ta@B_{20}^- boron drum with the record coordination number of twenty. *Chem. Commun.* **2017**, *53*, 1587–1590. [CrossRef]
17. Martínez-Guajardo, G.; Cabellos, J.L.; Díaz-Celaya, A.; Pan, S.; Islas, R.; Chattaraj, P.K.; Heine, T.; Merino, G. Dynamical behavior of borospherene: A nanobubble. *Sci. Rep.* **2015**, *5*, 11287. [CrossRef]
18. Guo, J.-C.; Feng, L.-Y.; Wang, Y.-J.; Jalife, S.; Vásquez-Espinal, A.; Cabellos, J.L.; Pan, S.; Merino, G.; Zhai, H.-J. Coaxial triple-layered versus helical $Be_6B_{11}^-$ clusters: Dual structural fluxionality and multifold aromaticity. *Angew. Chem. Int. Ed. Engl.* **2017**, *56*, 10174–10177. [CrossRef]
19. Feng, L.-Y.; Guo, J.-C.; Li, P.-F.; Zhai, H.-J. Boron-based binary $Be_6B_{10}^{2-}$ cluster: Three-layered aromatic sandwich, electronic transmutation, and dynamic structural fluxionality. *Phys. Chem. Chem. Phys.* **2018**, *20*, 22719–22729. [CrossRef]
20. Wang, Y.-J.; Feng, L.-Y.; Zhai, H.-J. Sandwich-type $Na_6B_7^-$ and $Na_8B_7^+$ clusters: Charge-transfer complexes, four-fold π/σ aromaticity, and dynamic fluxionality. *Phys. Chem. Chem. Phys.* **2019**, *21*, 18338–18345. [CrossRef]
21. Barroso, J.; Pan, S.; Merino, G. Structural transformations in boron clusters induced by metal doping. *Chem. Soc. Rev.* **2022**, *51*, 1098–1123. [CrossRef]
22. Yu, R.; Barroso, J.; Wang, M.-H.; Liang, W.-Y.; Chen, C.; Zarate, X.; Orozco-Ic, M.; Cui, Z.-H.; Merino, G. Structure and bonding of molecular stirrers with formula $B_7M_2^-$ and B_8M_2 (M = Zn, Cd, Hg). *Phys. Chem. Chem. Phys.* **2020**, *22*, 12312–12320.
23. Wen, L.; Zhou, D.; Yang, L.-M.; Li, G.; Ganz, E. Atomistic structures, stabilities, electronic properties, and chemical bonding of boron–aluminum mixed clusters $B_3Al_n^{0/-/+}$ (n = 2–6). *J. Cluster Sci.* **2021**, *32*, 1261–1276.
24. Ortiz-Chi, F.; Merino, G. *A Hierarchical Algorithm for Molecular Similarity (H-FORMS)*; GLOMOS: Mérida, Mexico, 2020.
25. Grande-Aztatzi, R.; Martínez-Alanis, P.R.; Cabellos, J.L.; Osorio, E.; Martínez, A.; Merino, G. Structural evolution of small gold clusters doped by one and two boron atoms. *J. Comput. Chem.* **2014**, *35*, 2288–2296. [CrossRef]
26. Adamo, C.; Barone, V. Toward reliable density functional methods without adjustable parameters: The PBE0 model. *J. Chem. Phys.* **1999**, *110*, 6158–6170.
27. Dunning, T.H., Jr.; Hay, P.J. *Modern Theoretical Chemistry*; Schaefer, H.F., III, Ed.; Plenum: New York, NY, USA, 1977; Volume 3, pp. 1–28.
28. Weigend, F.; Ahlrichs, R. Balanced basis sets of split valence, triple zeta valence and quadruple zeta valence quality for H to Rn: Design and assessment of accuracy. *Phys. Chem. Chem. Phys.* **2005**, *7*, 3297–3305.
29. Purvis, G.D., III; Bartlett, R.J. A full coupled-cluster singles and doubles model: The inclusion of disconnected triples. *J. Chem. Phys.* **1982**, *76*, 1910–1918.
30. Glendening, E.D.; Landis, C.R.; Weinhold, F. NBO 6.0: Natural bond orbital analysis program. *J. Comput. Chem.* **2013**, *34*, 1429–1437. [CrossRef]
31. Wiberg, K.B. Application of the pople-santry-segal CNDO method to the cyclopropylcarbinyl and cyclobutyl cation and to bicyclobutane. *Tetrahedron* **1968**, *24*, 1083–1096.
32. Millam, J.M.; Bakken, V.; Chen, W.; Hase, W.L.; Schlegel, H.B. Ab initio classical trajectories on the Born-Oppenheimer surface: Hessian-based integrators using fifth-order polynomial and rational function fits. *J. Chem. Phys.* **1999**, *111*, 3800–3805. [CrossRef]

33. Jusélius, J.; Sundholm, D.; Gauss, J. Calculation of current densities using gauge-including atomic orbitals. *J. Chem. Phys.* **2004**, *121*, 3952–3963. [CrossRef] [PubMed]
34. Fliegl, H.; Taubert, S.; Lehtonen, O.; Sundholm, D. The gauge including magnetically induced current method. *Phys. Chem. Chem. Phys.* **2011**, *13*, 20500–20518. [CrossRef] [PubMed]
35. Sundholm, D.; Fliegl, H.; Berger, R.J.F. Calculations of magnetically induced current densities: Theory and applications. *Wiley Interdiscip. Rev. Comput. Mol. Sci.* **2016**, *6*, 639–678. [CrossRef]
36. Sundholm, D.; Dimitrova, M.; Berger, R.J.F. Current density and molecular magnetic properties. *Chem. Commun.* **2021**, *57*, 12362–12378. [CrossRef] [PubMed]
37. Merino, G.; Heine, T.; Seifert, G. The induced magnetic field in cyclic molecules. *Chem.-Eur. J.* **2004**, *10*, 4367–4371. [CrossRef] [PubMed]
38. Heine, T.; Islas, R.; Merino, G. σ and π contributions to the induced magnetic field: Indicators for the mobility of electrons in molecules. *J. Comput. Chem.* **2007**, *28*, 302–309. [CrossRef] [PubMed]
39. Islas, R.; Heine, T.; Merino, G. The induced magnetic field. *Acc. Chem. Res.* **2012**, *45*, 215–228. [CrossRef]
40. Orozco-Ic, M.; Cabellos, J.L.; Merino, G. *Aromagnetic*; Cinvestav-Mérida: Mérida, Mexico, 2016.
41. Becke, A.D. A new mixing of Hartree-Fock and local density-functional theories. *J. Chem. Phys.* **1993**, *98*, 1372–1377. [CrossRef]
42. Lehtola, S.; Dimitrova, M.; Fliegl, H.; Sundholm, D. Benchmarking magnetizabilities with recent density functionals. *J. Chem. Theory Comput.* **2021**, *17*, 1457–1468. [CrossRef]
43. Ditchfield, R. Self-consistent perturbation theory of diamagnetism. *Mol. Phys.* **1974**, *27*, 789–807. [CrossRef]
44. Wolinski, K.; Hinton, J.F.; Pulay, P. Efficient implementation of the gauge-independent atomic orbital method for NMR chemical shift calculations. *J. Am. Chem. Soc.* **1990**, *112*, 8251–8260. [CrossRef]
45. Frisch, M.J.; Trucks, G.W.; Schlegel, H.B.; Scuseria, G.E.; Robb, M.A.; Cheeseman, J.R.; Scalmani, G.; Barone, V.; Mennucci, B.; Petersson, G.A.; et al. *Gaussian 16, Revision C.01*; Gaussian, Inc.: Wallingford, CT, USA, 2016.
46. Zubarev, D.Y.; Boldyrev, A.I. Developing paradigms of chemical bonding: Adaptive natural density partitioning. *Phys. Chem. Chem. Phys.* **2008**, *10*, 5207–5217. [CrossRef] [PubMed]
47. Lu, T.; Chen, F. Multiwfn: A multifunctional wavefunction analyzer. *J. Comput. Chem.* **2012**, *33*, 580–592. [CrossRef] [PubMed]
48. Cervantes-Navarro, F.; Martínez-Guajardo, G.; Osorio, E.; Moreno, D.; Tiznado, W.; Islas, R.; Donald, K.J.; Merino, G. Stop rotating! One substitution halts the B_{19}^- motor. *Chem. Commun.* **2014**, *50*, 10680–10682. [CrossRef]
49. Berger, R.J.F.; Dimitrova, M.; Nasibullin, R.T.; Valiev, R.R.; Sundholm, D. Integration of global ring currents using the Ampère-Maxwell law. *Phys. Chem. Chem. Phys.* **2022**, *24*, 624–628. [CrossRef]